V-ATPase Disassembly at the Yeast Lysosome-Like Vacuole Is a Phenotypic Driver of Lysosome Dysfunction in Replicative Aging

Fiza Hashmi and Patricia M. Kane

Department of Biochemistry and Molecular Biology
SUNY Upstate Medical University, Syracuse, NY USA

Address correspondence to: Patricia M. Kane
kanepm@upstate.edu

Running title: V-ATPase disassembly in replicative aging

Declines in lysosomal acidification and function with aging are observed in organisms ranging from yeast to humans. V-ATPases play a central role in organelle acidification and V-ATPase activity is regulated by reversible disassembly in many different settings. Using the yeast *Saccharomyces cerevisiae* as a replicative aging model, we demonstrate that V-ATPases disassemble into their V_1 and V_0 subcomplexes in aging cells, with release of V_1 subunit C (Vma5) from the lysosome-like vacuole into the cytosol. Disassembly is observed after ≥5 cell divisions and results in overall vacuole alkalinization. Caloric restriction, an established mechanism for reversing many age-related outcomes, prevents V-ATPase disassembly in older cells and preserves vacuolar pH homeostasis. Reversible disassembly is controlled in part by the activity of two opposing and conserved factors, the RAVE complex and Oxr1. The RAVE complex promotes V-ATPase assembly and a *rav1*Δ mutant shortens replicative lifespan; Oxr1 promotes disassembly and an *oxr1*Δ mutation extends lifespan. Importantly, the level of Rav2, a subunit of the RAVE complex, declines in aged cells, and Rav2 overexpression delays V-ATPase disassembly with age. These data indicate that reduced V-ATPase assembly contributes to the loss of lysosome acidification with age, which affects replicative lifespan.

Keywords: Aging, lysosomes, proton pumps, Saccharomyces cerevisiae, caloric restriction

22 **INTRODUCTION**

23 Lysosomal acidification is compromised with age in many organisms (Nixon, 2020).
24 Reduced acidification has multiple downstream functional consequences. Lysosomal hydrolases
25 operate optimally at the acidic pH, so cargo degradation is compromised at higher pH (Vilchez,
26 Saez, & Dillin, 2014). Lysosomes are terminal compartments for autophagy pathways, so
27 clearance of autophagic cargoes and recycling of nutrients, both critical in aging cells, is slowed
28 (Hansen, Rubinsztein, & Walker, 2018; Kaushik et al., 2021). Iron and other heavy metals are
29 sequestered in the acidic lysosomes; loss of sequestration can induce both oxidative stress (Diab
30 & Kane, 2013) and deficiency in mitochondrial iron-sulfur proteins (Chen et al., 2020). Reduced
31 lysosomal storage can also create toxic imbalances in amino acids such as cysteine that
32 contribute to loss of mitochondrial function (C. E. Hughes et al., 2020). Recent work highlights
33 the central role of the lysosome in nutritional signaling; many aspects of this signaling are linked
34 to acidification (Perera & Zoncu, 2016). Loss of lysosomal acidification impacts many processes
35 associated with age-related functional decline, but the mechanisms behind increased lysosomal
36 pH are not fully understood.

37 The highly conserved vacuolar H^+- ATPase (V-ATPase) acidifies lumens of lysosomes
38 and lysosome-like vacuoles, as well as endosomes and the late Golgi apparatus (Collins &
39 Forgac, 2020). V-ATPases are multi-subunit protein complexes that couple ATP hydrolysis to
40 proton pumping into organelle lumens. The V-ATPase consists of two subcomplexes: a
41 peripheral V_1 subcomplex that is responsible for ATP hydrolysis connected to a membrane-
42 embedded V_0 subcomplex containing the proton pore. V-ATPase subunit sequences are
43 conserved across eukaryotes and recent V-ATPase structures indicate very strong structural
44 similarity between yeast and mammalian V-ATPases (Oot & Wilkens, 2020).

45 V-ATPase activity is highly regulated and responsive to environmental conditions.
46 Reversible disassembly is a versatile mechanism of V-ATPase regulation that fine-tunes the
47 activity of the proton pump to meet cellular demands (Collins & Forgac, 2020; Jaskolka,
48 Winkley, & Kane, 2021). In reversible disassembly, the V_1 subcomplex is released from the V_0
49 subcomplex inhibiting both ATP hydrolysis and proton pumping (Kane, 1995; Sumner et al.,
50 1995). V_1 subunit C dissociates from both subcomplexes and becomes cytosolic during
51 disassembly (Kane, 1995). Disassembly is post-translational and rapidly reversible (Kane,
52 1995). It was first observed in the yeast *S. cerevisiae* and the tobacco hornworm *M. sexta* upon
53 acute glucose deprivation and was reversed by glucose replenishment (Kane, 1995; Sumner et
54 al., 1995). It has since become clear that reversible disassembly occurs widely and in response to
55 diverse signals. For example, many cells appear to promote V-ATPase reassembly under
56 conditions of nutrient deprivation and mTOR inhibition, possibly as a means of promoting
57 lysosomal proteolysis and nutrient recycling (Ratto et al., 2022). In neurons, V-ATPases are
58 reversibly disassembled as part of each synaptic vesicle cycle (Bodzeta, Kahms, & Klingauf,
59 2017). In cardiomyocytes, lipid overload can promote V-ATPase disassembly in endosomes,
60 ultimately contributing to long-term insulin resistance (Liu et al., 2017). Reversible disassembly
61 can also be manipulated by both host cells and pathogens to prevent or facilitate infection (Kohio
62 & Adamson, 2013).
63 The RAVE (Regulator of Acidification of Vacuoles and Endosomes) complex and TLDc
64 (Tre2/Bub2/Cdc16 LysM domain catalytic) protein Oxr1 regulate reversible disassembly of the
65 V-ATPase (Jaskolka, Winkley, et al., 2021; Khan et al., 2022; Klossel et al., 2024; Seol,
66 Shevchenko, & Deshaies, 2001). The RAVE complex consists of three subunits: Rav1, Rav2, and
67 Skp1 and is required for reassembly of V-ATPase complexes disassembled by glucose

68 deprivation. In mutants lacking Rav1 or Rav2, V-ATPases are disassembled into V_1 and V_0
69 subcomplexes and vacuolar acidification is lost (Jaskolka, Winkley, et al., 2021). The role of
70 Skp1 in RAVE is less clear and it may be dispensable for RAVE function (Jaskolka, Winkley, et
71 al., 2021). The RAVE complex associates with V_1 subcomplexes in the cytosol (Jaskolka,
72 Tarsio, Smardon, Khan, & Kane, 2021). In contrast, recent studies suggest that Oxr1, a member
73 of the TLDc family of proteins, promotes disassembly of V-ATPases. Mutants lacking Oxr1
74 maintain higher levels of assembled V-ATPases in the absence of glucose (Khan et al., 2022;
75 Khan & Wilkens, 2024; Klossel et al., 2024).

76 Several mechanisms for loss of lysosomal acidification with age have been proposed. In
77 yeast, the long-lived plasma membrane proton pump, Pma1, accumulates in mother cells, and it
78 has been proposed that increased proton export through Pma1 disrupts the balance of Pma1 and
79 V-ATPase activities and compromises organelle acidification (Devare et al., 2020; Henderson,
80 Hughes, & Gottschling, 2014). Early loss of vacuolar acidification in yeast has been correlated
81 with defective mitochondrial morphology and function. Both vacuolar deacidification and
82 mitochondrial morphology phenotypes are suppressed by overexpression of the V-ATPase
83 catalytic subunit, *VMA1*, or an ER-localized assembly factor, *VPH2 (VMA12)*, suggesting a
84 possible deficiency in these factors with age (A. L. Hughes & Gottschling, 2012). In *C. elegans*,
85 stability of the *VMA1* transcript is controlled by a microRNA, miR-1, which can globally control
86 lysosomal acidification (Schiffer et al., 2021). Wilms et al. (Wilms et al., 2017) demonstrated
87 that deletion of the mTOR effector Sch9 promotes V-ATPase assembly and extends yeast
88 chronological lifespan (CLS). All of these mechanisms could contribute to loss of
89 vacuolar/lysosomal acidification.

90 However, despite the importance of reversible disassembly in V-ATPase regulation, V-
91 ATPase assembly state during aging has not been explored extensively. Here we show that V-
92 ATPase assembly changes with age in a yeast replicative aging model. Increased V-ATPase
93 disassembly in older cells is accompanied by decreased vacuolar acidification that does not
94 appear to stem from reduced V-ATPase subunit levels. Instead, we provide evidence that reduced
95 activity of the RAVE (Regulator of H^+-ATPase of Vacuolar and Endosomal membranes)
96 assembly complex may give rise to net V-ATPase disassembly and increased lysosomal pH with
97 age.
98

99 **RESULTS**

100 *V-ATPases are more disassembled and vacuoles more alkaline after ~5 cell divisions.*

101 Given the evidence that vacuoles and lysosomes are less acidic in older cells, we
102 hypothesized that V-ATPase assembly and activity might also change with age. Replicative aging
103 in the yeast *S. cerevisiae* is a widely accepted model for aging (He, Zhou, & Kennedy, 2018).
104 Yeast cells divide asymmetrically with each cell division giving rise to a new, "rejuvenated"
105 daughter cell from an established mother cell. Each cell division leaves a bud scar on the mother,
106 allowing visual assessment of age. The yeast V_1C subunit (Vma5) is released from both V_1 and
107 V_0 during V-ATPase disassembly, so we first visualized Vma5-GFP localization in a mixed age
108 population of cells (Figure 1). (Vacuoles are visible as indentations under DIC (differential
109 interference contrast) optics.) In parallel, we monitored replicative age of each cell by staining
110 with calcofluor white (CW) which labels the bud scars on mother cells. As shown in Figure 1a,
111 Vma5-GFP is tightly localized to the vacuolar membrane in cells with few or no bud scars. In
112 contrast, in older cells with more bud scars, Vma5-GFP exhibited a marked decrease in
113 fluorescence at the vacuolar membrane and a notable increase in cytosolic fluorescence. To
114 compare Vma5-GFP localization between cells, we quantitated maximum fluorescence from a
115 line scan across each cell. As shown in Figure 1b, a line scan from a young cell has prominent
116 peaks corresponding to edges of the vacuole with a high maximum fluorescence signal, while
117 older cells have less prominent peaks. We conducted the same analysis across populations of
118 cells of mixed age, normalized to the maximum fluorescence signal of young cells and binned
119 the results by the number of bud scars. As shown in Figure 1c, young cells, defined as having
120 less than 5 bud scars, displayed Vma5-GFP localization at the vacuolar membrane. However, the
121 normalized maximum fluorescence signal, representative of vacuole localization, decreases

122 significantly in cells with five bud scars or more. This early onset of V-ATPase disassembly
123 aligns with previous reports indicating declines in lysosomal pH early in replicative aging (A. L.
124 Hughes & Gottschling, 2012).

125 Vma5 is a V_1 subunit that bridges the V_1 and V_0 subcomplexes of the V-ATPase. The V_1
126 subcomplex also contains Vma2, and the V_0 subcomplex contains Vph1, which comprises part of
127 the proton pore (Figure 2a). Vma5 appears to be released most completely from the membrane
128 by reversible disassembly (Tabke et al., 2014), but the rest of V_1 also dissociates from the
129 vacuolar membrane. We assessed the cellular distribution of Vma2-GFP and Vph1-GFP. There
130 was less membrane-bound Vma2-GFP in older cells relative to younger cells (Figure 2b), when
131 assessed as in Figure 1. However, vacuolar Vph1-GFP levels were the same between old and
132 young cells (Figure 2c). These results are consistent with disassembly of the V-ATPase as cells
133 age.

134 Although comparable levels of Vph1 at the vacuole suggests that expression of V_0
135 subunits and V_0 assembly are intact, V_1 subunits could become cytosolic because of reduced V_1
136 subunit levels in older cells. To address this question, we isolated populations old and young
137 yeast cells by biotinylating the cell walls in a mixed age population, allowing growth to continue
138 for several generations, and then obtaining "old" cells by biotin-streptavidin affinity
139 chromatography (Jin, Cao, & Liu, 2021). Daughter cells that emerged after biotinylation cannot
140 bind to magnetic streptavidin beads and represent the "young" population. The age distribution
141 was determined by counting bud scars in each population and binning by the number of buds per
142 cell (Figure 2d). When prepared by this method, the population of old cells peaks at 20-24 bud
143 scars, while there was a median value of 0-4 bud scars in the young population. Cell lysates were
144 prepared from each population and analyzed by SDS-PAGE and immunoblotting. As shown in

145 Figures 2e and f, there is no significant difference in the cellular levels of V_1 subunits Vma1,
146 Vma2, and Vma5 between young and old populations. These results indicate that the cytosolic
147 populations of V_1 subunits arise from disassembly of the V-ATPase, rather than inability to
148 assemble because of lack of V-ATPase subunits.

149 Reversible disassembly of V-ATPases is employed in a number of contexts to provide
150 dynamic regulation of the complex in response to changing cellular conditions. Disassembled V_1
151 and V_0 subcomplexes lack ATPase and proton transport activity and ATP-driven proton pumping
152 is restored upon reassembly. In order to test whether the lower levels of assembled V-ATPases in
153 old cells result in reduced capacity for acidification, we measured the response of young and old
154 cells to an acute glucose deprivation (an abrupt shift to 0% glucose), which promotes
155 disassembly of the yeast V-ATPase, followed by readdition of glucose to a 2% final
156 concentration, which promotes reassembly and reactivation of the complex (Kane, 1995).

157 Young and old yeast cells obtained as described above were loaded with the ratiometric
158 pH sensor BCECF-AM (2',7'-Bis-(2-carboxyethyl)-5-(and-6)-carboxyfluorescein acetoxy methyl
159 ester) which localizes to the vacuole in yeast cells (Diakov, Tarsio, & Kane, 2013). Both young
160 and old cells were shifted to medium with no glucose for ~30 minutes. Fluorescence of cell
161 suspensions was then monitored continuously (Figure 3a) and glucose was added at the indicated
162 time. This assay revealed clear age-dependent differences in the vacuolar pH response to glucose
163 stimulation. Young cells exhibit a rapid drop in vacuolar pH upon glucose addition. This drop
164 was previously shown to be V-ATPase-dependent and to correlate with V-ATPase assembly
165 (Martinez-Munoz & Kane, 2008). In old cells, however, there was a smaller pH decrease after
166 glucose addition, indicating a more alkaline vacuole and consistent with the lower levels of V-
167 ATPase assembly observed by microscopy during growth in glucose-replete media in Figures 1

168 and 2. Quantitative analysis of pH at defined time points across biological replicates (Figure 3b)
169 indicates that vacuoles in old cells are significantly more alkaline than their younger counterparts
170 at each of the indicated time points. These results suggest an age-related alteration in vacuolar
171 pH regulation through the inability of V-ATPase to reassemble. As a result, vacuoles in old cells
172 display a more alkaline pH than vacuoles in young cells.

173 *Caloric restriction restores V-ATPase assembly and vacuolar acidification in older cells.*

174 Caloric restriction (CR) is defined as a reduction in caloric intake in the presence of
175 adequate nutrition (Longo & Anderson, 2022). CR promotes both cellular health and longevity.
176 Extensive research in organisms ranging from yeast to worms, flies, and rodents suggests that
177 CR can have significant anti-aging effects and promote overall health (Longo & Anderson,
178 2022). For *S. cerevisiae*, adjusting the concentration of glucose in the growth medium from the
179 2% used above to 0.5% is a common way to induce CR. This treatment does not significantly
180 reduce growth rate over several cell divisions (Supporting information Figure 1a).

181 As shown in Figure 4, CR reverses the V-ATPase disassembly in older cells. Notably, the
182 V_1 subunits Vma5-GFP (Figure 4a) and Vma2-GFP (Figure 4b) are recruited to the vacuolar
183 membrane in both young and old cells, and there is no significant difference in fluorescence at
184 the vacuolar membrane with age. Fluorescence intensities of Vph1-GFP continue to be similar
185 between old and young cells (Figure 4c). This suggests that CR extends V-ATPase assembly
186 beyond the replicative age of $\geq$5 bud scars when cells grown in higher glucose begin to show
187 disassembly.

188 We hypothesized that vacuolar pH in old cells might also be restored. We grew cells
189 under CR conditions and monitored vacuolar pH before and after addition of glucose as
190 described above. Figure 4d demonstrates that the glucose-stimulated decrease in vacuolar pH,

191 which was compromised in older cells grown in 2% glucose (Figure 3), was restored to the level
192 of young cells in cells after growth under CR conditions. This observation indicates that CR has
193 a direct impact on both V-ATPase assembly and vacuolar acidification in aging cells. In addition,
194 it further highlights the potential connection between V-ATPase assembly, vacuolar acidification
195 and aging.

196 These results point to nutritional signaling as an important determinant of V-ATPase
197 assembly and activity in aging cells. Bond and Forgac demonstrated that V-ATPase assembly
198 was preserved under low glucose conditions in an *ira2*Δ mutant. Deletion of *IRA2*, or its
199 paralogue *IRA1*, activates the Ras/protein kinase A (PKA) pathway (Bond & Forgac, 2008). We
200 hypothesized that V-ATPase assembly might be preserved in older cells, mimicking the effects of
201 CR, in an *ira2*Δ mutant. We visualized Vma5-GFP localization and as shown in Supporting
202 Information Figure 1b, the *ira2*Δ cells do maintain V-ATPase assembly in older cells. Therefore,
203 we determined replicative lifespan (RLS) for the *ira2*Δ mutant by daughter dissection
204 (Supporting Information Figure 1c). The median lifespan of the *ira2*Δ mutant is significantly
205 shorter than that of wild-type cells. These data are consistent with evidence that upregulation of
206 the Ras/protein kinase A pathway shortens lifespan (Longo & Anderson, 2022) and suggest that
207 although there is improved V-ATPase assembly in older cells in the *ira2*Δ mutant, it is not
208 sufficient to balance effects on other targets of the pathway in aging cells.

209 *Regulators of V-ATPase assembly affect replicative lifespan.*

210 We next sought to manipulate V-ATPase assembly more directly in order to assess the
211 significance of maintaining V-ATPase assembly and activity in aging cells. We hypothesized
212 that the RAVE complex and Oxr1, cellular factors that promote V-ATPase assembly and
213 disassembly as shown in Figure 5a, might also affect RLS.

214 To explore the functional significance of these assembly regulators in aging cells, we
215 examined the RLS of deletion mutants lacking Rav1 or Oxr1 (Figure 5b). RLS was measured at
216 pH 5, conditions that are optimal for growth of *rav1*Δ strains. Deletion of Rav1 shortened RLS
217 (median 17 cell divisions, n= 30) by 26% relative to wild-type cells (median 23 cell divisions, n=
218 30). In contrast, the *oxr1*Δ mutation extended RLS by 47.8% over wild-type (median 34 cell
219 divisions, n=30). These results reinforce the significance of V-ATPase assembly in RLS and
220 suggest that the RAVE pro-assembly activity (disrupted in the *rav1*Δ mutant) and Oxr1 anti-
221 assembly activity (lost in *oxr1*Δ) may be central determinants of lifespan.

222 We next asked whether loss of RAVE and Oxr1 affects chronological aging of yeast cells.
223 Replicative aging assesses the number of times a mother cells can divide, while chronological
224 aging assesses cell survival as nutrients are depleted over time. Wild-type cells and *rav1*Δ,
225 *oxr1*Δ, and *vma1*Δ mutants were grown to saturation in medium buffered to pH 5.5 (Murakami et
226 al., 2012; Wilms et al., 2017). (*VMA1* encodes the catalytic subunit of the V-ATPase and the
227 *vma1*Δ mutant has no V-ATPase activity.). At the indicated times, aliquots were removed from
228 each culture, cell density was determined, and a defined number of cells was plated on fresh
229 medium. The percentage of each cell type that formed colonies (c.f.u.) on fresh plates at each
230 time is shown in Figure 5c. Even in buffered medium, which improves the survival of *vma*
231 mutants (Wilms et al., 2017), less than half of the *vma1*Δ and *rav1*Δ mutant cells are able to form
232 colonies after 2 weeks. In contrast, almost half of the *oxr1*Δ cells form colonies at 4 weeks, and
233 wild-type cells have an intermediate phenotype. The percentage of cells staining with propidium
234 iodide, an indication of cell permeabilization and death, increases as colony formation declines
235 (Figure 5d). However, it is notable that even after 5 weeks, only ~60% of *oxr1*Δ cells stain with
236 propidium iodide. These results complement the replicative aging data and indicate that

237 mutations that preserve V-ATPase assembly can significantly increase lifespan, while mutations
238 that compromise activity and/or assembly decrease lifespan. Yeast encode a second isoform of
239 the V_0 a-subunit, Stv1, which localizes to the Golgi in wild-type cells. Stv1-containing V-
240 ATPases do not require RAVE for assembly (Smardon et al., 2014), and Stv1 has been shown to
241 relocalize to the vacuole in an *oxr1*Δ mutant (Klossel et al., 2024). In order to test whether the
242 lifespan extension in *oxr1*Δ cells arises from Stv1-containing V-ATPases at the vacuole, we
243 constructed a *stv1*Δ*oxr1*Δ double mutant strain and assessed its RLS and V-ATPase assembly. As
244 shown in Supporting Information Figure 2a, the double mutant strain retains the long lifespan of
245 the *oxr1*Δ relative to wild-type, suggesting that vacuolar Stv1 is not responsible for this effect.
246 Rather, V-ATPases containing the Vph1 isoform account for the assembly in older cells of the
247 *oxr1*Δ mutant (Supplemental Information Figure 2b).

248 Given the results with these deletion mutants, we asked whether there were differences in
249 levels of the RAVE subunits or Oxr1 between young and old cells. We isolated young and old
250 populations of cells containing functional myc13-tagged Rav1 or FLAG-tagged Rav2 by
251 biotinylation and streptavidin magnetic separation as described above (Figure 2), then assessed
252 the levels of the tagged proteins in cell lysates. Although there is no significant difference in
253 Rav1-myc13 levels between young and old cells (Figure 6a), we consistently observed a
254 significant decrease in the level of Rav2-FLAG in older cells (Figure 6b). We assessed
255 expression of *RAV2* in young and old cells by quantitative PCR but observed no difference in
256 mRNA levels (Supporting Information Figure 2c). Because Rav2 is required for RAVE complex
257 function in promoting V-ATPase assembly (Seol et al., 2001; Smardon, Tarsio, & Kane, 2002),
258 these results suggest that partial loss of RAVE function in old cells could contribute to reduced
259 V-ATPase assembly and replicative aging. We transformed the cells containing a chromosomal

260 copy of Rav2-FLAG with an additional copy of Rav2-FLAG on a low-copy plasmid to
261 determine whether we could increase Rav2 levels and improve V-ATPase assembly in older cells.
262 As shown in Figure 6b, addition of the plasmid increases Rav2-FLAG levels in old cells. We
263 compared Vma5-GFP localization with and without the Rav2-FLAG plasmid in a mixed age
264 population in Figure 6c. In cells overexpressing Rav2-FLAG, Vma5-GFP is at higher levels in
265 the vacuoles of cells with ≥5 bud scars. The quantitation and binning by bud scar number in
266 Figure 6d confirms that there is no significant decline in vacuolar Vma5-GFP in cells with 5-9
267 bud scars and only in cells with ≥ 15 bud scars does vacuolar fluorescence reach the level in
268 "old" wild-type cells (Figure 1). These data indicate that increasing Rav2-FLAG levels can help
269 preserve V-ATPase assembly in older cells.

270 We hypothesized that restoration of V-ATPase assembly in older cells grown under CR
271 conditions (Figure 4) might be supported by restoration of Rav2 levels. To test this, we isolated
272 young and old populations from Rav2-myc13 tagged cells grown under CR conditions. Under
273 these conditions, V-ATPase assembly and function is restored in older cells (Figure 4) and Rav2
274 levels are also restored (Figure 6e).

275 Alterations in Oxr1 levels with age could also affect V-ATPase assembly. We isolated
276 young and old populations from a strain containing HA-tagged Oxr1 and found that the levels of
277 Oxr1-HA in whole cell lysates do not change with age (Figure 6f). To further explore the basis of
278 the extended RLS in *oxr1*Δ cells, we observed Vma5-GFP localization in a population of *oxr1*Δ
279 cells of mixed age. As shown in Figure 6g, h, *oxr1*Δ mutants localize Vma5-GFP to the vacuole
280 even in older cells with ≥5 bud scars. To quantitate this effect, we again binned cells by the
281 number of bud scars as described above, and compared Vma5-GFP localization to localization in

young daughter cells (Figure 6h). In contrast to wild-type cells, there is no significant difference in Vma5-GFP localization in the *oxr1*Δ mutant until cells have divided 25 or more times.

Intriguingly, these results suggest that the *oxr1*Δ mutation mirrors the effects of CR on V-ATPase assembly and longevity. The results also indicate that direct manipulation of V-ATPase assembly by mutation of critical assembly factors can affect replicative and chronological lifespan, both of which are linked to cellular pH homeostasis (Murakami et al., 2012). Specifically, promoting V-ATPase assembly through the RAVE complex appears to be important for preserving lifespan, while the opposing effects of Oxr1 on the V-ATPase tend to shorten lifespan.

DISCUSSION

These results establish V-ATPase disassembly as an important factor in reduced vacuolar acidification in aging cells. We demonstrate an increase in V-ATPase disassembly at relatively early replicative ages (5-9 cell divisions) similar to the age at which Hughes and Gottschling first observed compromised vacuolar acidification (A. L. Hughes & Gottschling, 2012). We show that promoting assembly of the V-ATPase through CR can restore V-ATPase assembly and vacuolar pH in older cells. Deletion of Oxr1, a negative regulator of V-ATPase assembly, can extend both replicative and chronological lifespan. In contrast, mutation of the RAVE complex shortens lifespan and levels of the Rav2 subunit decline with age. Taken together, these data support V-ATPase disassembly as a significant age-related factor behind reduced vacuolar and lysosomal acidification and the associated declines in function.

This mechanism does not necessarily conflict with those proposed previously. If V-ATPases are more disassembled in older cells, cells may be less able to tolerate an imbalance

305 between Pma1 activity at the plasma membrane and V-ATPase activity at the vacuole
306 (Henderson et al., 2014). Okreglak et al. (Okreglak et al., 2023) recently visualized oscillations
307 of vacuolar pH in mother cells that were coordinated with cell cycle. Oscillations cease upon V-
308 ATPase inhibition, but it is not clear whether reversible disassembly of the V-ATPase is required.
309 It is possible that this oscillatory behavior is lost in older mother cells, leading to loss of their
310 ability to restore vacuolar pH after cell division. Notably, we see no difference in protein levels
311 of V_1 subunits Vma1, Vma2, and Vma5, between young and old cells. The similar levels of
312 Vph1 in vacuoles of young and old cells suggest that V_0 subunits are present at similar levels,
313 since V_0 assembly occurs in the ER and reduced levels of any V_0 subunit reduces V_0 subcomplex
314 levels at the vacuole. The data presented here suggest a post-transcriptional regulatory
315 mechanism, but increased levels of a biosynthetic assembly factor (A. L. Hughes & Gottschling,
316 2012) could promote assembly and improve acidification.

317 Many questions remain to be investigated. The reduction in Rav2 protein levels with age
318 appears to be post-transcriptional but we do not yet know whether this arises from reduced
319 translation or increased degradation. It is intriguing in young cells, addition of an extra copy of
320 Rav2-FLAG did not increase levels of the protein in Figure 6b, suggesting the Rav2 subunit
321 levels are controlled. Perhaps more importantly, even though reduced levels of Rav2 levels helps
322 explain increased V-ATPase disassembly and addition of extra Rav2 improves assembly, we do
323 not know whether the Rav2 reduction occurs as a result of some general vulnerability in aging
324 cells or is deliberately programmed (Gladyshev et al., 2021). The significant increase in lifespan
325 and prolonged V-ATPase assembly in *oxr1*Δ cells seems to argue against any growth advantage
326 from increased V-ATPase disassembly in older cells, at least at the single cell level.

327 Many aging pathways are tightly linked to nutritional signaling, and reversible
328 disassembly is often driven by nutritional signaling pathways. Given the rapid disassembly of the
329 V-ATPase upon acute glucose deprivation (Kane, 1995), it was initially surprising that growth
330 under CR conditions suppresses V-ATPase disassembly with age. However, we previously
331 showed that the acute disassembly response required glucose concentrations well below 0.5%
332 (Parra & Kane, 1998). Activation of the PKA pathway in the *ira2*Δ mutant (Supporting
333 Information Figure 1b) promotes V-ATPase assembly in older cells, but also results in a decrease
334 in RLS. In mammalian cells, V-ATPase assembly generally increases in response to nutrient
335 deprivation or inhibition of mTOR function (Ratto et al., 2022). CR could mimic this effect in
336 aging cells, preserving lysosomal acidification and function. Deletion of the mTOR effector
337 *SCH9* extends RLS and CLS and promotes V-ATPase assembly (Wilms et al., 2017), similar to
338 the effect of *oxr1*Δ mutation. Signals involved in reversible disassembly of the V-ATPase are
339 incompletely understood and vary between physiological settings (Collins & Forgac, 2020). The
340 RAVE complex responds to nutritional signals associated with reversible disassembly with
341 release from the vacuolar membrane upon acute glucose deprivation and recruitment to the
342 membrane upon glucose restoration, even in the absence of V_1 subunit C and the V_1 subcomplex
343 (Jaskolka, Winkley, et al., 2021). The molecular mechanism of Oxr1-induced V-ATPase
344 assembly is understood (Khan & Wilkens, 2024), but its response to cellular signaling is still
345 being explored.

346 Reduced V-ATPase assembly could be a factor in the age-related decline in lysosomal
347 acidification and function in higher eukaryotes. Reversible disassembly occurs in higher
348 eukaryotes including mammalian cells. Rabconnectin-3 complexes of higher eukaryotes are
349 functional homologues of the yeast RAVE complex (Jaskolka, Winkley, et al., 2021). Oxr1

350 belongs to a family of TLDc proteins and several of these proteins have been shown to bind to
351 mammalian V-ATPases and induce disassembly (Oot & Wilkens, 2024). These data suggest that
352 the core elements for controlled V-ATPase disassembly during aging are present in other cells.
353 We observed V-ATPase disassembly in a yeast replicative aging model, which is most
354 comparable to mammalian cell types that continue to divide, such as adult stem cells (He et al.,
355 2018), and observed similar effects of *rav1*Δ and *oxr1*Δ mutations in chronological aging, which
356 is more analogous to long-lived, non-dividing mammalian cells. Taken together, these data
357 suggest that V-ATPase assembly state is linked to different types of aging and could easily play a
358 role in aging in higher eukaryotes.

359 **METHODS**

360 *Yeast strains and plasmids*

361 All strains analyzed were in the BY4741 (*MATa his3Δ1 leu2Δ0 met15Δ0 ura3Δ0*) or BY4742
362 (*MATα his3Δ1 leu2Δ0 lys1Δ ura3Δ0*) background. BY4742 strains containing Vma5-GFP::*HIS3*
363 and Vph1-GFP::*HIS3* were constructed as part of the genome-wide GFP-tagging project (Huh et
364 al., 2003). The *rav1*Δ*::kanMX, oxr1*Δ*::kanMX, vma1*Δ*::kanMX*, and *ira2*Δ*::kanMX* mutant
365 strains in the BY4741 background were purchased as part of a haploid deletion collection.
366 *VMA2* was C-terminally tagged with GFP by PCR amplification from pFA6a-GFP-KanMX6 and
367 genomic integration (Longtine et al., 1998). The *oxr1*Δ*::kanMX* Vma5-GFP::*HIS3* strain was
368 obtained by crossing BY4741 *oxr1*Δ*::kanMX* and BY4742 Vma5-GFP::*HIS3* and obtaining
369 spores with the desired genotype by tetrad dissection. The *stv1*Δ*::natMX* mutation was
370 introduced by crossing this strain to a *stv1*Δ*::natMX* haploid and sporulating. The pRS316 Oxr1-
371 HA plasmid (Khan & Wilkens, 2024) was transformed into *oxr1Δ::kanMX* and transformants
372 were selected on medium lacking uracil. Rav1-myc13::*kanMX*, Rav2-myc13::*kanMX*, and Rav2-

373 FLAG::*kanMX* strains were constructed as described previously (Jaskolka, Tarsio, et al., 2021;
374 Smardon et al., 2002). The tagged alleles were PCR amplified from the original strains and
375 integrated into BY4741.

376 *Fluorescence microscopy*

377 Strains expressing GFP-tagged Vma5, Vma2, or Vph1 were grown to log phase in
378 synthetic complete (SC) medium containing either 2% or 0.5% glucose overnight, pelleted by
379 centrifugation, then suspended in fresh medium containing 2% or 0.5% glucose and grown for an
380 additional 2 hours. Cells were stained by addition of CW (final concentration 10 μg/ml) 5 min
381 prior to imaging. Cells were visualized with a 100x oil (NA 1.4) objective on a Zeiss Imager.Z1
382 fluorescence microscope with a Hamamastu CCD camera and AxioVision software. Cells were
383 viewed through DIC optics and fluorescence was imaged using a DAPI filter set (for CW) and a
384 GFP filter set. Bud scars were counted from CW staining; in mixed age populations, cells with 5
385 or more bud scars were designated as old and those with less than 5 as young. To obtain a more
386 precise count of bud scars for binning, cells were visualized on multiple focal planes. GFP
387 fluorescence images were captured for cells in each binned range then processed in FIJI. To
388 assess vacuolar localization, a line was drawn across a cell and through the vacuolar membrane.
389 From this line scan, a plot illustrating fluorescence intensity along the line was generated, with
390 peaks indicating areas of elevated fluorescence at the vacuolar membrane. The peak intensity
391 (maximum fluorescence) was quantitated as a measure of vacuolar localization. Each biological
392 replicate corresponds to a distinct culture of yeast cells. Maximum fluorescence was quantitated
393 for at least 20 young and 20 old cells per biological replicate. In cells were binned by age, at
394 least 20 cells per biological replicate were counted for each bin. Maximum fluorescence from
395 line scans of young and old cells in each biological replicate were averaged and then divided by

396 the average for young cells in that replicate to normalize. Normalized fluorescence for each
397 biological replicate was plotted, along with average intensities across replicates +/- s.e.m.
398 (standard error of the mean). Statistical significance was determined by t-test for the young and
399 old cell comparisons and by ANOVA for binned samples. To show the range of values for the
400 young cells across experiments, the values for young cells across biological replicates were
401 averaged; individual replicates were divided by this average are shown as points on each graph.

402 *Age Enrichment*

403 Age enrichment was performed as described by Jin et al. (Jin et al., 2021). Cells were collected
404 from a 50 mL fresh overnight culture in YEP (yeast extract-peptone medium) supplemented with
405 2% or 0.5% glucose to an OD_{600} of 1.0 and washed twice with cold phosphate-buffered saline
406 (PBS), pH 7.4. Cells were pelleted by centrifugation and washed three times in cold sterile PBS,
407 then labeled with 1.6 mg/ml EZ-Link Sulfo-NHS-LC-Biotin (Pierce) at room temperature for 30
408 min with gentle agitation. After labeling, the cells were washed three times with cold PBS, pH
409 8.0, to remove free biotin, and resuspended in YEP medium supplemented with 2% or 0.5%
410 glucose for growth overnight. After 16 hours, cells were pelleted by centrifugation and
411 resuspended in 35 ml of cold PBS, pH 7.4, mixed with 250 µl of a magnetic streptavidin bead
412 suspension (Pierce), and incubated for 60 min at 4°C. The mixture, in a 50 mL conical tube, was
413 loaded onto a magnetic separation column (Permagen) at 4°C to separate biotinylated cells.
414 Unbound (young) cells were removed gently by pipetting. Magnetically separated cells were
415 subsequently washed three times by resuspending in 35 mL PBS, pH 7.4 supplemented with 2%
416 or 0.5% glucose, repeating magnetic separation, and discarding the supernatant. After washing,
417 cells were resuspended in 200 mL of YEP or SC containing 2% or 0.5% glucose and allowed to
418 grow for an additional 4 hours before obtaining the final "old" mother cells and "young"

419 daughter cells. Cells were loaded on the magnetic separation column as described above and
420 daughter cells obtained from the supernatant were pelleted by centrifugation to obtain a
421 concentrated population of young cells. After the final wash, the magnetic beads were
422 resuspended in 1 ml PBS, pH 7.4 and centrifuged to concentrate the old population. The two
423 populations were then used immediately for pH measurements or stored at -80°C for further
424 biochemical analysis.

425 *Whole Cell Lysates and Immunoblots*

426 Cell pellets from age-enriched young and old cell populations were resuspended in
427 cracking buffer (8 M urea, 5% SDS, 1 mM EDTA, 50 mM Tris-HCl, pH 6.8) at 95°C and lysed
428 with glass beads. Cellular debris was pelleted by centrifugation at 16,000 × g for 2 min, and
429 supernatants containing whole-cell extracts were used immediately or stored at −80 °C until use.

430 After determination of protein concentrations by Bradford assay, equal amounts of
431 protein were separated by SDS-PAGE and transferred to a nitrocellulose membrane. Blots were
432 blocked, then incubated overnight with primary antibodies at 4°C. Primary antibodies (all at a
433 1:500 dilution) included mouse monoclonal antibodies 7A2 against Vma5, 10D7 against Vph1,
434 8B1 against Vma1, and 13D11 against Vma2 (Kane, Kuehn, Howald-Stevenson, & Stevens,
435 1992). In addition, anti-myc monoclonal 9E10 (Santa Cruz Biotechnology), anti-HA monoclonal
436 (BioLegend), anti-FLAG (Sigma) and anti-GAPDH (Proteintech) antibodies were used at 1:500,
437 1:500, 1:1000, and 1:10,000 dilution, respectively. HRP-conjugated anti-mouse secondary
438 antibody (Bio-Rad) was added at a final dilution of 1:2000 and incubated for 60 min at room
439 temperature. The blot was washed, incubated with Bio-Rad Clarity Western ECL substrate and
440 imaged in an Azure Sapphire FL Biomolecular Imager. Images were quantified using FIJI.

441 Molecular mass markers were included on every blot. In blot images, the nearest molecular mass
442 marker is indicated.

443 *Vacuolar pH Measurements*

444 Vacuolar pH was measured using BCECF-AM (Invitrogen) as described previously (Diakov et
445 al., 2013). Age-enriched populations of cells were loaded with BCECF-AM in YEP
446 supplemented with 2% or 0.5% glucose. After washing with YEP media to remove dye, cells
447 were resuspended in YEP, deprived of glucose, and incubated for 30 min. For fluorescence
448 measurement, 20 µl of cell suspension was diluted into 3 ml 1 mM 2-(N-
449 morpholino)ethanesulfonic acid (MES) pH 5.0 buffer, and fluorescence intensity at excitation
450 wavelengths 450 and 495 nm and emission wavelength 535 nm and was monitored continuously
451 in a Horiba Jovin Yvon Spectrafluor Max fluorometer at 30°C. The fluorescence ratio for each
452 sample was calibrated in every experiment by clamping pH in the range of 5.0 to 7.0 and
453 constructing a calibration curve.

454 *Replicative Life Span*

455 RLS was determined on YEP, 2% glucose plates buffered to pH 5. Daughter cells were
456 sequentially removed by micromanipulation (Steffen, Kennedy, & Kaeberlein, 2009). Survival
457 curves are pooled data from experiment-matched controls. The number of divisions for 26-30
458 mother cells were scored for each curve. p-values for replicative life span survival curve
459 comparisons were calculated with a Cox regression model. Kaplan-Meier survival curves were
460 plotted with GraphPad Prism.

461 *Chronological lifespan analysis*

462 CLS was assessed as described (Wilms et al., 2017), with the following modifications. Cells
463 were pre-cultured to the stationary phase in SC containing 2% glucose. Stationary-phase cells

464 were then diluted to an OD_{600} of 0.1 in fresh medium and grown for 48 hours; the end of this
465 time is designated as time zero. Cells were aged in SC containing 2% glucose adjusted to pH 5.5
466 with 500 mM MES. Cell viability and clonogenicity (colony forming units; CFUs) were
467 analyzed on days 7, 14, 21, 28, and 35. Cell death was assessed by propidium iodide staining
468 (Sigma) and visualized by fluorescence microscopy. For CFU analysis, cell density was
469 measured using a hemocytometer, and 250 cells were plated onto YPD plates. After incubation,
470 CFUs were counted using FIJI, and the results expressed as the percentage of total cells plated.
471 Statistical significance was assessed by ANOVA with multiple sequence comparisons (GraphPad
472 Prism).

473 *RT-PCR of RAV2 from young and old cells*

474 RNA was extracted from young and old cells, obtained by age enrichment as described above,
475 using the NEB Monarch Total RNA Miniprep Kit. RT-PCR was conducted using the NEB Luna
476 Universal One-Step RT-qPCR Kit and performed on a Bio-Rad CFX384 Touch System. Data
477 analysis was conducted using CFX Maestro Software.

478

479 **Acknowledgements**: This work was supported by NIH R35 GM145256 to P.M.K. The authors
480 thank M. Murad Khan and Dr. Stephan Wilkens for sharing the *oxr1*Δ strain and Oxr1-HA
481 plasmid, and Dr. Xin Jie Chen for helpful discussions and a critical reading of the manuscript.
482 Illustrations in Figures 2a and 5a were prepared using Biorender.com.

483 **Author contributions**: F.H. performed experiments, analyzed data, prepared figures, and wrote
484 the first draft of the manuscript; P.M.K. obtained funding for the project, analyzed data, prepared
485 figures, and contributed to writing of the manuscript.

Conflict of interest: The authors declare that they have no conflicts of interest with the contents of this article.

Data availability: The data that support the findings of this study are available at Upstate.figshare.com. https://upstate.figshare.com. DOI: 10.58120/upstate.27902313

491 **FIGURE LEGENDS**

492 **Figure 1: V-ATPases are more disassembled in yeast cells of older replicative age. (a)** Vma5-
493 GFP cells grown in SC containing 2% glucose. DIC was used to visualize vacuoles. Bud scars
494 are stained with CW to determine replicative age. **(b)** Left panel provides representative example
495 of quantitative measurements using line scans. The young and old cells are from the dashed
496 white and red boxes, respectively, in the Vma5-GFP image of **Figure 1a**. Plot profiles are
497 superimposed for the young (black) and old (red) cells. **(c)** Quantitation of maximum fluorescent
498 intensity across five biological replicates, after normalization to the average intensity in the
499 youngest bin for each replicate. Each biological replicate (dot) represents at least 20 cells and
500 bars represent the mean +/- s.e.m. "Old" for subsequent experiments (without age enrichment) is
501 categorized as ≥5 bud scars. **** represents a p-value <0.0001 calculated by ordinary one-way
502 ANOVA.

503 **Figure 2: Age-enriched populations of cells have comparable levels of V-ATPase subunits.**
504 **(a)** Diagram of V-ATPase showing the positions of Vma5, Vma2, and Vph1. **(b)** Vma2-GFP cells
505 (V_1B) grown in SC with 2% glucose. CW was used to visualize bud scars. The CW images for
506 young cells were overexposed relative to those for the old cells in order to visualize the low level
507 staining in young cells. Normalized maximum fluorescence was obtained as in **Figure 1**. Means
508 +/- s.e.m. of three biological replicates are shown; each replicate is represented by a dot.
509 Significance was assessed by unpaired Student's *t* test, *** p value=0.0009 . **(c)** Vph1-GFP cells
510 were visualized and analyzed as described in **2b**. **(d)** After biotin-streptavidin age enrichment,
511 bud scars were counted for 100 cells in young and old populations, then binned by bud count. **(e)**
512 Lysates from age-enriched populations defined as in **1c** were separated by SDS-PAGE.
513 Immunoblots for the indicated proteins in young (Y) vs. old (O) cell populations as defined as in

514 **1c**. **(f)** Band intensities were quantified using FIJI, ratios of subunit levels to the GAPDH control
515 were calculated and normalized to the young population for each biological replicate. Data are
516 presented as mean (horizontal bars) ± s.e.m. (whiskers) of three biological replicates. n.s.= not
517 significant by unpaired Student's *t* test.
518
519 **Figure 3: Vacuolar pH is more alkaline in old cells. (a)** Vacuolar pH responses were measured
520 for wild-type BY4742 age-enriched young and old populations as described in Methods.
521 Glucose-deprived cultures were loaded with BCECF-AM. Fluorescence intensity values were
522 collected every 10 sec and glucose was added to a final concentration of 2% after 3 min. The
523 ratio of fluorescence signals was converted to pH as described in Methods. **(b)** pH measurements
524 at 1 min (before glucose addition), 5 min (2 min after glucose addition), and 8 min (5 min after
525 addition) are presented as mean (horizontal bars) ± s.e.m. (whiskers) of three biological
526 replicates. * = p value of 0.02, ** p value <0.001.
527
528 **Figure 4: Caloric restriction restores V-ATPase assembly and vacuolar pH in old cells. (a-c)**
529 Strains used in **Figures 1** and **2** show recruitment of Vma5-GFP (**a)** and Vma2-GFP **(b)** to the
530 vacuolar membrane after growth in SC with 0.5% glucose. Vph1-GFP (**c)** remains unchanged.
531 Normalized maximum fluorescence was quantitated as described in Methods. No significant
532 differences between young and old cells were observed by unpaired Student's *t* test. Designation
533 of young and old cells by CW staining was as described in **Figure 1**. **(d)** Young and old cell
534 populations were obtained by biotin-streptavidin age-enrichment from cells grown in YEP
535 supplemented with 0.5% glucose, and vacuolar pH responses were measured. Data were

536 collected and analyzed as in **Figure 3b**. Data are presented as mean (horizontal bars) ± s.e.m.
537 (whiskers) of three biological replicates.
538
539 **Figure 5: Effects of *rav1*Δ and *oxr1*Δ on RLS and CLS. (a)** Schematic of reversible
540 disassembly. **(b)** Kaplan-Meier curves comparing the RLS of *rav1*Δ (green), *oxr1*Δ (red), and
541 wild-type cells (black). Median number of replicative generations is shown in parentheses, with
542 the % difference between median values for *rav1*Δ and *oxr1*Δ vs. wild-type. Deletion of *OXR1*
543 increases RLS ($p<0.001$), and deletion of RAVE component *RAV1* shortens RLS ($p < 0.01$). **(c,**
544 **d)** Plots of colony-forming units **(c)** and percentage of cells stained with propidium iodide **(d)** vs.
545 time. Each point is the mean of three biological replicates. Strains included are defined to the
546 right of **(c)**. Statistical analysis of **(c)** indicates a p-value <0.0001 for all mutants in comparison
547 to wild-type. In **(d)**, *vma1*Δ and *oxr1*Δ differed from wild-type with a p-value <0.0001, and
548 *rav1*Δ with a p-value= 0.0007.
549
550 **Figure 6: RAVE subunit and Oxr1 levels in aging cells. (a)** Rav1 levels in young and old cells.
551 Age-enriched populations were obtained from WT cells containing Rav1-myc_{13} (young (Y)
552 versus old (O) cells). Cell lysates were prepared and analyzed as in **Figure 2**. Normalized data
553 are presented as mean (horizontal bars) ± s.e.m. (whiskers) of three biological replicates. ns=not
554 significant. **(b)** Rav2-FLAG levels from young and old cells prepared as in **6a** from haploid cells
555 containing only a chromosomally integrated (int.) Rav2-FLAG or cells with both integrated
556 Rav2-FLAG and low copy Rav2-FLAG plasmid (+plasmid). Normalized data are presented as
557 mean (horizontal bars) ± s.e.m. (whiskers) of three biological replicates. ****, p-value<0.0001,
558 ns= not significant. **(c)** Rav2-FLAG Vma5-GFP cells, without (int.) or with the Rav2-FLAG

559 plasmid (+ plasmid). CW is used to visualize bud scars as in **Figure 1**; white stars on the Vma5-
560 GFP images indicate newborn cells with no bud scars. Images representative of cells with 0-4,
561 5-9, and 10-14 bud scars are shown. **(d)** Rav2-FLAG cells + plasmid were binned by the number
562 of bud scars and normalized maximal fluorescence quantitated as in **Figure 1**. **, p-value<0.01
563 and *, p-value<0.05 for the indicated comparisons; n.s.=not significant. **(e)** Immunoblot analysis
564 comparing Rav2-myc_{13} levels in cells grown in YEP with 2% glucose or 0.5% glucose (CR
565 conditions). Samples were prepared, analyzed, and presented as in **6a**. ***, p- value <0.001,
566 n.s.= not significant. **(f)** Immunoblot of lysates from *oxr1Δ* strain expressing Oxr1-HA from a
567 low copy plasmid. Young and old cells were isolated as in **6a**. Data are presented as mean
568 (horizontal bars) ± s.e.m. (whiskers) of three biological replicates. **(g)** Wild-type and *oxr1Δ* cells
569 containing Vma5-GFP grown in SC with 2% glucose. DIC and CW were used to visualize
570 vacuoles and bud scars as in **Figure 2b**. **(h)** *oxr1*Δ cells were binned by the number of bud scars
571 and normalized maximal fluorescence quantitated as in **Figure 1**. ***, p-value <0.001 in
572 comparison to the youngest bin; there is no other significant difference.
573

574 **REFERENCES**
575

576 Bodzeta, A., Kahms, M., & Klingauf, J. (2017). The Presynaptic v-ATPase Reversibly
577 Disassembles and Thereby Modulates Exocytosis but Is Not Part of the Fusion Machinery.
578 *Cell Rep, 20*(6), 1348-1359. doi:10.1016/j.celrep.2017.07.040
579 Bond, S., & Forgac, M. (2008). The Ras/cAMP/protein kinase A pathway regulates glucose-
580 dependent assembly of the vacuolar (H+)-ATPase in yeast. *J Biol Chem, 283*(52), 36513-
581 36521. doi:M805232200 [pii]10.1074/jbc.M805232200
582 Chen, K. L., Ven, T. N., Crane, M. M., Brunner, M. L. C., Pun, A. K., Helget, K. L., . . . Wasko, B.
583 M. (2020). Loss of vacuolar acidity results in iron-sulfur cluster defects and divergent
584 homeostatic responses during aging in Saccharomyces cerevisiae. *Geroscience, 42*(2), 749-
585 764. doi:10.1007/s11357-020-00159-3
586 Collins, M. P., & Forgac, M. (2020). Regulation and function of V-ATPases in physiology and
587 disease. *Biochim Biophys Acta Biomembr, 1862*(12), 183341.
588 doi:10.1016/j.bbamem.2020.183341
589 Devare, M. N., Kim, Y. H., Jung, J., Kang, W. K., Kwon, K. S., & Kim, J. Y. (2020). TORC1
590 signaling regulates cytoplasmic pH through Sir2 in yeast. *Aging Cell, 19*(6), e13151.
591 doi:10.1111/acel.13151
592 Diab, H. I., & Kane, P. M. (2013). Loss of vacuolar H+-ATPase (V-ATPase) activity in yeast
593 generates an iron deprivation signal that is moderated by induction of the peroxiredoxin
594 TSA2. *Journal of Biological Chemistry, 288*(16), 11366-11377. doi:M112.419259 [pii]
595 10.1074/jbc.M112.419259
596 Diakov, T. T., Tarsio, M., & Kane, P. M. (2013). Measurement of vacuolar and cytosolic pH in
597 vivo in yeast cell suspensions. *J Vis Exp, Apr 19*(74). doi:10.3791/50261
598 Gladyshev, V. N., Kritchevsky, S. B., Clarke, S. G., Cuervo, A. M., Fiehn, O., de Magalhaes, J. P.,
599 . . . Cummings, S. R. (2021). Molecular Damage in Aging. *Nat Aging, 1*(12), 1096-1106.
600 doi:10.1038/s43587-021-00150-3
601 Hansen, M., Rubinsztein, D. C., & Walker, D. W. (2018). Autophagy as a promoter of longevity:
602 insights from model organisms. *Nat Rev Mol Cell Biol, 19*(9), 579-593.
603 doi:10.1038/s41580-018-0033-y
604 He, C., Zhou, C., & Kennedy, B. K. (2018). The yeast replicative aging model. *Biochim Biophys*
605 *Acta Mol Basis Dis, 1864*(9 Pt A), 2690-2696. doi:10.1016/j.bbadis.2018.02.023
606 Henderson, K. A., Hughes, A. L., & Gottschling, D. E. (2014). Mother-daughter asymmetry of pH
607 underlies aging and rejuvenation in yeast. *Elife, 3*, e03504. doi:10.7554/eLife.03504
608 Hughes, A. L., & Gottschling, D. E. (2012). An early age increase in vacuolar pH limits
609 mitochondrial function and lifespan in yeast. *Nature, 492*(7428), 261-265. doi:nature11654
610 [pii]10.1038/nature11654
611 Hughes, C. E., Coody, T. K., Jeong, M. Y., Berg, J. A., Winge, D. R., & Hughes, A. L. (2020).
612 Cysteine Toxicity Drives Age-Related Mitochondrial Decline by Altering Iron
613 Homeostasis. *Cell, 180*(2), 296-310 e218. doi:10.1016/j.cell.2019.12.035
614 Huh, W. K., Falvo, J. V., Gerke, L. C., Carroll, A. S., Howson, R. W., Weissman, J. S., & O'Shea,
615 E. K. (2003). Global analysis of protein localization in budding yeast. *Nature, 425*(6959),
616 686-691.
617 Jaskolka, M. C., Tarsio, M., Smardon, A. M., Khan, M. M., & Kane, P. M. (2021). Defining steps
618 in RAVE-catalyzed V-ATPase assembly using purified RAVE and V-ATPase
619 subcomplexes. *J Biol Chem, 296*, 100703. doi:10.1016/j.jbc.2021.100703

Jaskolka, M. C., Winkley, S. R., & Kane, P. M. (2021). RAVE and Rabconnectin-3 Complexes as Signal Dependent Regulators of Organelle Acidification. *Front Cell Dev Biol, 9*, 698190. doi:10.3389/fcell.2021.698190

Jin, X., Cao, X., & Liu, B. (2021). Isolation of Aged Yeast Cells Using Biotin-Streptavidin Affinity Purification. *Methods Mol Biol, 2196*, 223-228. doi:10.1007/978-1-0716-0868-5_17

Kane, P. M. (1995). Disassembly and reassembly of the yeast vacuolar H(+)-ATPase in vivo. *J Biol Chem, 270*(28), 17025-17032.

Kane, P. M., Kuehn, M. C., Howald-Stevenson, I., & Stevens, T. H. (1992). Assembly and targeting of peripheral and integral membrane subunits of the yeast vacuolar H(+)-ATPase. *J Biol Chem, 267*(1), 447-454.

Kaushik, S., Tasset, I., Arias, E., Pampliega, O., Wong, E., Martinez-Vicente, M., & Cuervo, A. M. (2021). Autophagy and the hallmarks of aging. *Ageing Res Rev, 72*, 101468. doi:10.1016/j.arr.2021.101468

Khan, M. M., Lee, S., Couoh-Cardel, S., Oot, R. A., Kim, H., Wilkens, S., & Roh, S. H. (2022). Oxidative stress protein Oxr1 promotes V-ATPase holoenzyme disassembly in catalytic activity-independent manner. *EMBO J, 41*(3), e109360. doi:10.15252/embj.2021109360

Khan, M. M., & Wilkens, S. (2024). Molecular mechanism of Oxr1p mediated disassembly of yeast V-ATPase. *EMBO Rep*. doi:10.1038/s44319-024-00126-5

Klossel, S., Zhu, Y., Amado, L., Bisinski, D. D., Ruta, J., Liu, F., & Gonzalez Montoro, A. (2024). Yeast TLDc domain proteins regulate assembly state and subcellular localization of the V-ATPase. *EMBO J*. doi:10.1038/s44318-024-00097-2

Kohio, H. P., & Adamson, A. L. (2013). Glycolytic control of vacuolar-type ATPase activity: a mechanism to regulate influenza viral infection. *Virology, 444*(1-2), 301-309. doi:S0042-6822(13)00396-6 [pii]
10.1016/j.virol.2013.06.026

Liu, Y., Steinbusch, L. K. M., Nabben, M., Kapsokalyvas, D., van Zandvoort, M., Schonleitner, P., . . . Luiken, J. (2017). Palmitate-Induced Vacuolar-Type H(+)-ATPase Inhibition Feeds Forward Into Insulin Resistance and Contractile Dysfunction. *Diabetes, 66*(6), 1521-1534. doi:10.2337/db16-0727

Longo, V. D., & Anderson, R. M. (2022). Nutrition, longevity and disease: From molecular mechanisms to interventions. *Cell, 185*(9), 1455-1470. doi:10.1016/j.cell.2022.04.002

Longtine, M. S., McKenzie, A., 3rd, Demarini, D. J., Shah, N. G., Wach, A., Brachat, A., . . . Pringle, J. R. (1998). Additional modules for versatile and economical PCR-based gene deletion and modification in Saccharomyces cerevisiae. *Yeast, 14*(10), 953-961.

Martinez-Munoz, G. A., & Kane, P. (2008). Vacuolar and plasma membrane proton pumps collaborate to achieve cytosolic pH homeostasis in yeast. *J Biol Chem, 283*(29), 20309-20319. doi:M710470200 [pii]
10.1074/jbc.M710470200

Murakami, C., Delaney, J. R., Chou, A., Carr, D., Schleit, J., Sutphin, G. L., . . . Kaeberlein, M. (2012). pH neutralization protects against reduction in replicative lifespan following chronological aging in yeast. *Cell Cycle, 11*(16), 3087-3096. doi:10.4161/cc.21465

Nixon, R. A. (2020). The aging lysosome: An essential catalyst for late-onset neurodegenerative diseases. *Biochim Biophys Acta Proteins Proteom, 1868*(9), 140443. doi:10.1016/j.bbapap.2020.140443

Okreglak, V., Ling, R., Ingaramo, M., Thayer, N. H., Millett-Sikking, A., & Gottschling, D. E. (2023). Cell cycle-linked vacuolar pH dynamics regulate amino acid homeostasis and cell growth. *Nat Metab, 5*(10), 1803-1819. doi:10.1038/s42255-023-00872-1

Oot, R. A., & Wilkens, S. (2020). A "Sugar-Coated" Proton Pump Comes into Focus: High-Resolution Structure of a Human V-ATPase. *Mol Cell, 80*(3), 379-380. doi:10.1016/j.molcel.2020.10.020

Oot, R. A., & Wilkens, S. (2024). Human V-ATPase function is positively and negatively regulated by TLDc proteins. *Structure, 32*(7), 989-1000 e1006. doi:10.1016/j.str.2024.03.009

Parra, K. J., & Kane, P. M. (1998). Reversible association between the V1 and V0 domains of yeast vacuolar H+-ATPase is an unconventional glucose-induced effect. *Mol Cell Biol, 18*(12), 7064-7074. Retrieved from http://mcb.asm.org/cgi/content/full/18/12/7064

Perera, R. M., & Zoncu, R. (2016). The Lysosome as a Regulatory Hub. *Annu Rev Cell Dev Biol, 32*, 223-253. doi:10.1146/annurev-cellbio-111315-125125

Ratto, E., Chowdhury, S. R., Siefert, N. S., Schneider, M., Wittmann, M., Helm, D., & Palm, W. (2022). Direct control of lysosomal catabolic activity by mTORC1 through regulation of V-ATPase assembly. *Nat Commun, 13*(1), 4848. doi:10.1038/s41467-022-32515-6

Schiffer, I., Gerisch, B., Kawamura, K., Laboy, R., Hewitt, J., Denzel, M. S., . . . Antebi, A. (2021). miR-1 coordinately regulates lysosomal v-ATPase and biogenesis to impact proteotoxicity and muscle function during aging. *Elife, 10*. doi:10.7554/eLife.66768

Seol, J. H., Shevchenko, A., & Deshaies, R. J. (2001). Skp1 forms multiple protein complexes, including RAVE, a regulator of V-ATPase assembly. *Nat Cell Biol, 3*(4), 384-391.

Smardon, A. M., Diab, H. I., Tarsio, M., Diakov, T. T., Nasab, N. D., West, R. W., & Kane, P. M. (2014). The RAVE complex is an isoform-specific V-ATPase assembly factor in yeast. *Mol Biol Cell, 25*(3), 356-367. doi:mbc.E13-05-0231 [pii]
10.1091/mbc.E13-05-0231

Smardon, A. M., Tarsio, M., & Kane, P. M. (2002). The RAVE complex is essential for stable assembly of the yeast V-ATPase. *J Biol Chem, 277*(16), 13831-13839.

Steffen, K. K., Kennedy, B. K., & Kaeberlein, M. (2009). Measuring replicative life span in the budding yeast. *J Vis Exp*(28). doi:10.3791/1209

Sumner, J. P., Dow, J. A., Earley, F. G., Klein, U., Jager, D., & Wieczorek, H. (1995). Regulation of plasma membrane V-ATPase activity by dissociation of peripheral subunits. *J Biol Chem, 270*(10), 5649-5653.

Tabke, K., Albertmelcher, A., Vitavska, O., Huss, M., Schmitz, H. P., & Wieczorek, H. (2014). Reversible disassembly of the yeast V-ATPase revisited under in vivo conditions. *Biochemical Journal, 462*(1), 185-197. doi:BJ20131293 [pii]
10.1042/BJ20131293

Vilchez, D., Saez, I., & Dillin, A. (2014). The role of protein clearance mechanisms in organismal ageing and age-related diseases. *Nat Commun, 5*, 5659. doi:10.1038/ncomms6659

Wilms, T., Swinnen, E., Eskes, E., Dolz-Edo, L., Uwineza, A., Van Essche, R., . . . Winderickx, J. (2017). The yeast protein kinase Sch9 adjusts V-ATPase assembly/disassembly to control pH homeostasis and longevity in response to glucose availability. *PLoS Genet, 13*(6), e1006835. doi:10.1371/journal.pgen.1006835

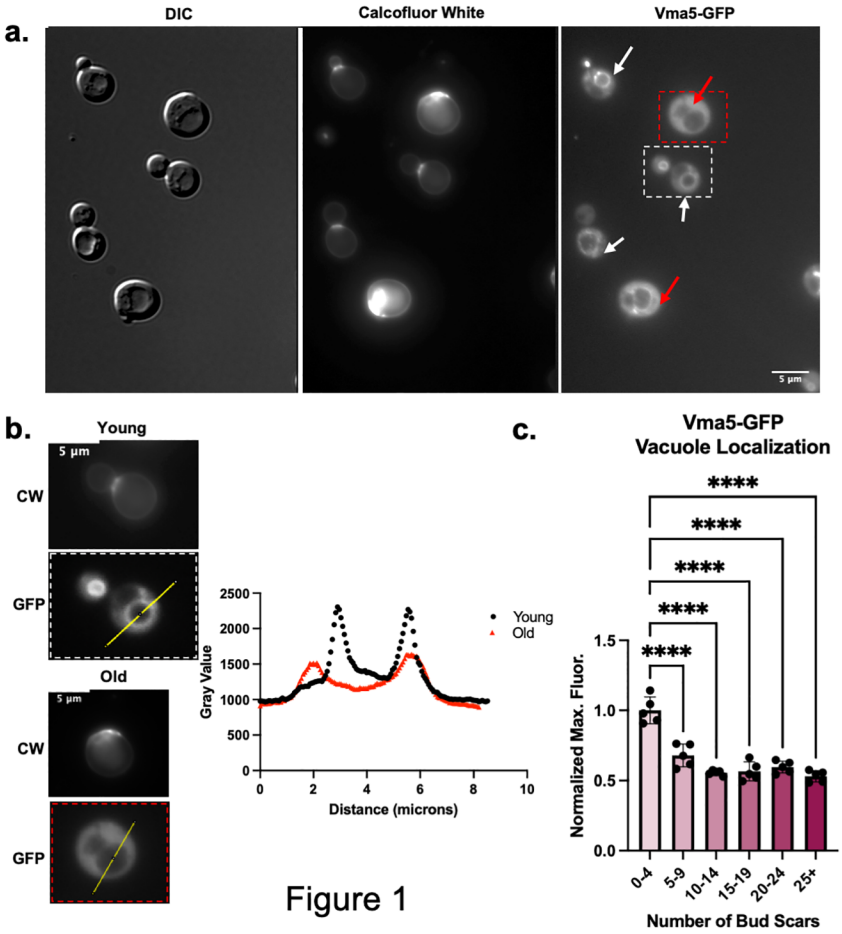
a.
DIC
Calcofluor White
Vma5-GFP
5 µm
b.
Young
5 µm
CW
GFP
Old
5 µm
CW
GFP
Gray Value
2500
2000
1500
1000
500
0
0
2
4
6
8
10
Distance (microns)
Young
Old
c.
Vma5-GFP
Vacuole Localization
****
****
****
****
****
Normalized Max. Fluor.
1.5
1.0
0.5
0.0
0-4
5-9
10-14
15-19
20-24
25+
Number of Bud Scars

Figure 1

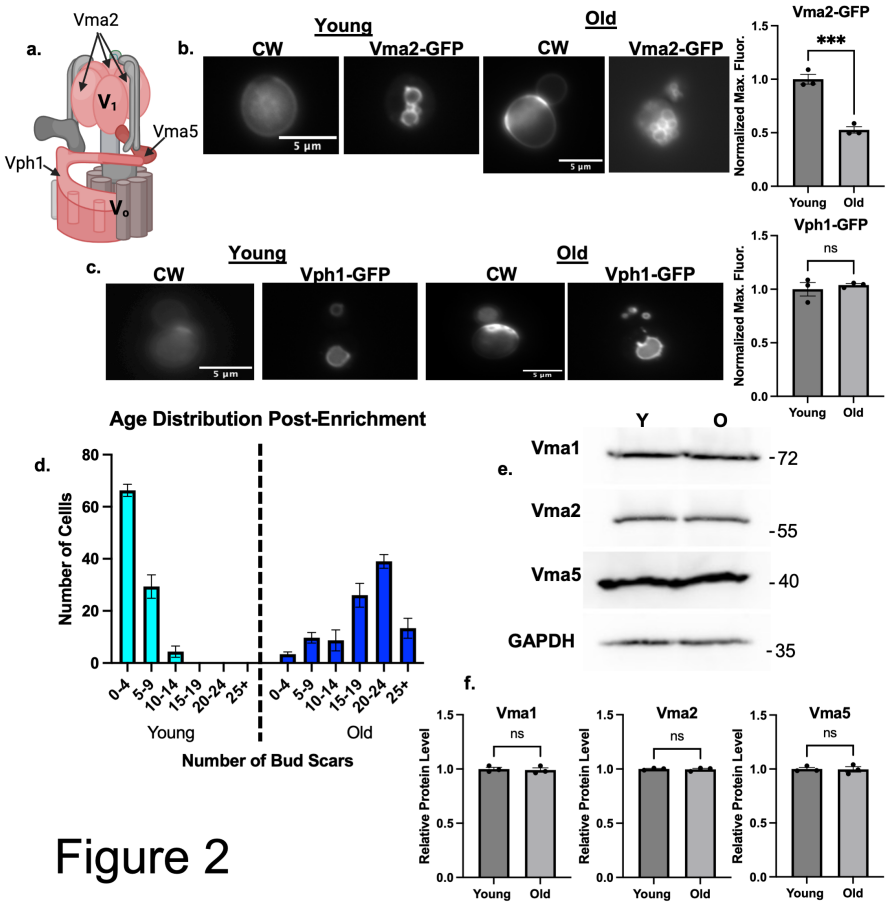
a.
Vma2
V1
Vma5
Vph1
Vo
b.
Young
Old
CW
Vma2-GFP
CW
Vma2-GFP
5 µm
Vma2-GFP
***
Normalized Max. Fluor.
Young
Old
c.
Young
Old
CW
Vph1-GFP
CW
Vph1-GFP
Vph1-GFP
ns
Normalized Max. Fluor.
Young
Old
Age Distribution Post-Enrichment
d.
Number of Cells
0-4
5-9
10-14
15-19
20-24
25+
Young
Old
Number of Bud Scars
e.
Y
O
Vma1
Vma2
Vma5
GAPDH
-72
-55
-40
-35
f.
Vma1
Vma2
Vma5
ns
Relative Protein Level
Young
Old

Figure 2

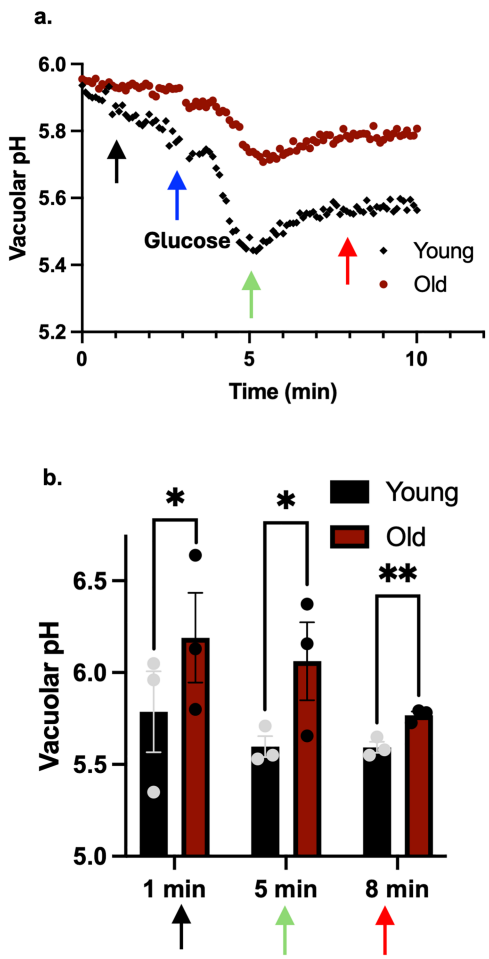
a.
6.0
5.8
5.6
5.4
5.2
Vacuolar pH
Glucose
Young
Old
0
5
10
Time (min)
b.
Young
Old
*
*
**
6.5
6.0
5.5
5.0
Vacuolar pH
1 min
5 min
8 min

Figure 3

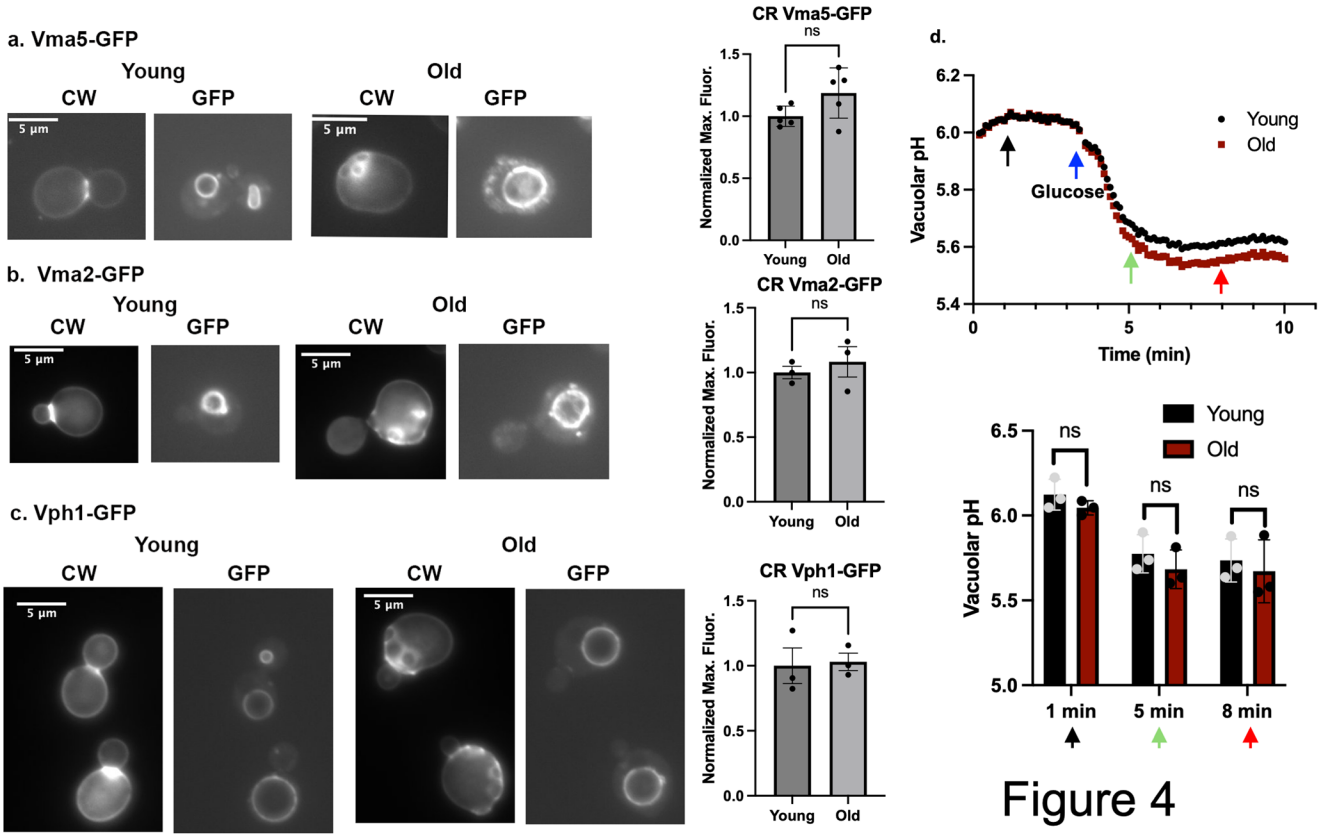
a. Vma5-GFP
Young
Old
CW
GFP
CW
GFP
5 µm
5 µm
b. Vma2-GFP
Young
Old
CW
GFP
CW
GFP
5 µm
5 µm
c. Vph1-GFP
Young
Old
CW
GFP
CW
GFP
5 µm
5 µm
CR Vma5-GFP
ns
Normalized Max. Fluor.
1.5
1.0
0.5
0.0
Young
Old
CR Vma2-GFP
ns
Normalized Max. Fluor.
1.5
1.0
0.5
0.0
Young
Old
CR Vph1-GFP
ns
Normalized Max. Fluor.
1.5
1.0
0.5
0.0
Young
Old
d.
Vacuolar pH
6.2
6.0
5.8
5.6
5.4
Glucose
Young
Old
0
5
10
Time (min)
Young
Old
Vacuolar pH
6.5
6.0
5.5
5.0
ns
ns
ns
1 min
5 min
8 min

Figure 4

Figure 5

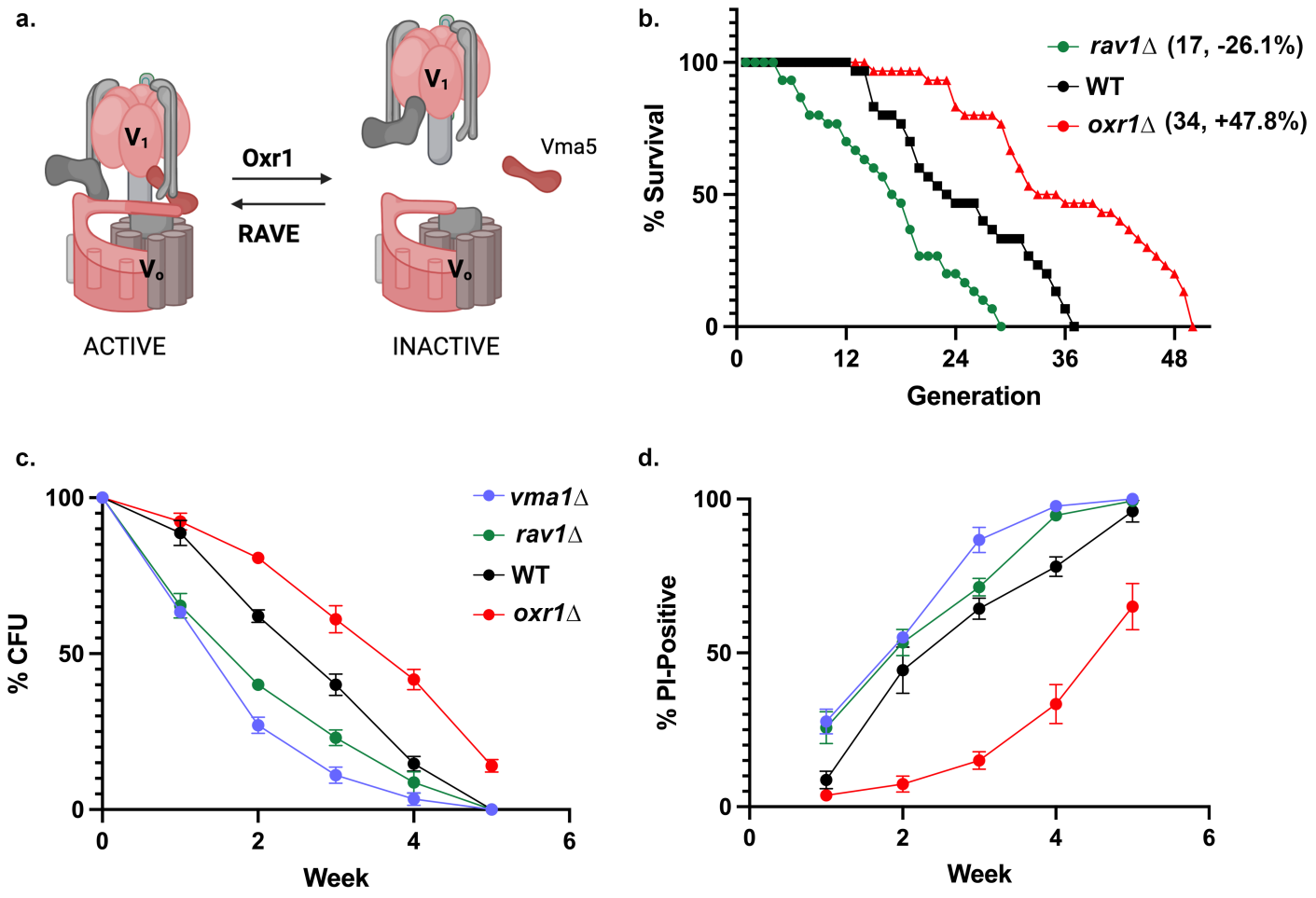
a.
V1
Vo
Oxr1
RAVE
V1
Vo
Vma5
ACTIVE
INACTIVE
b.
% Survival
100
50
0
0
12
24
36
48
Generation
rav1Δ (17, -26.1%)
WT
oxr1Δ (34, +47.8%)
c.
% CFU
100
50
0
0
2
4
6
Week
vma1Δ
rav1Δ
WT
oxr1Δ
d.
% PI-Positive
100
50
0
0
2
4
6
Week

Figure 6

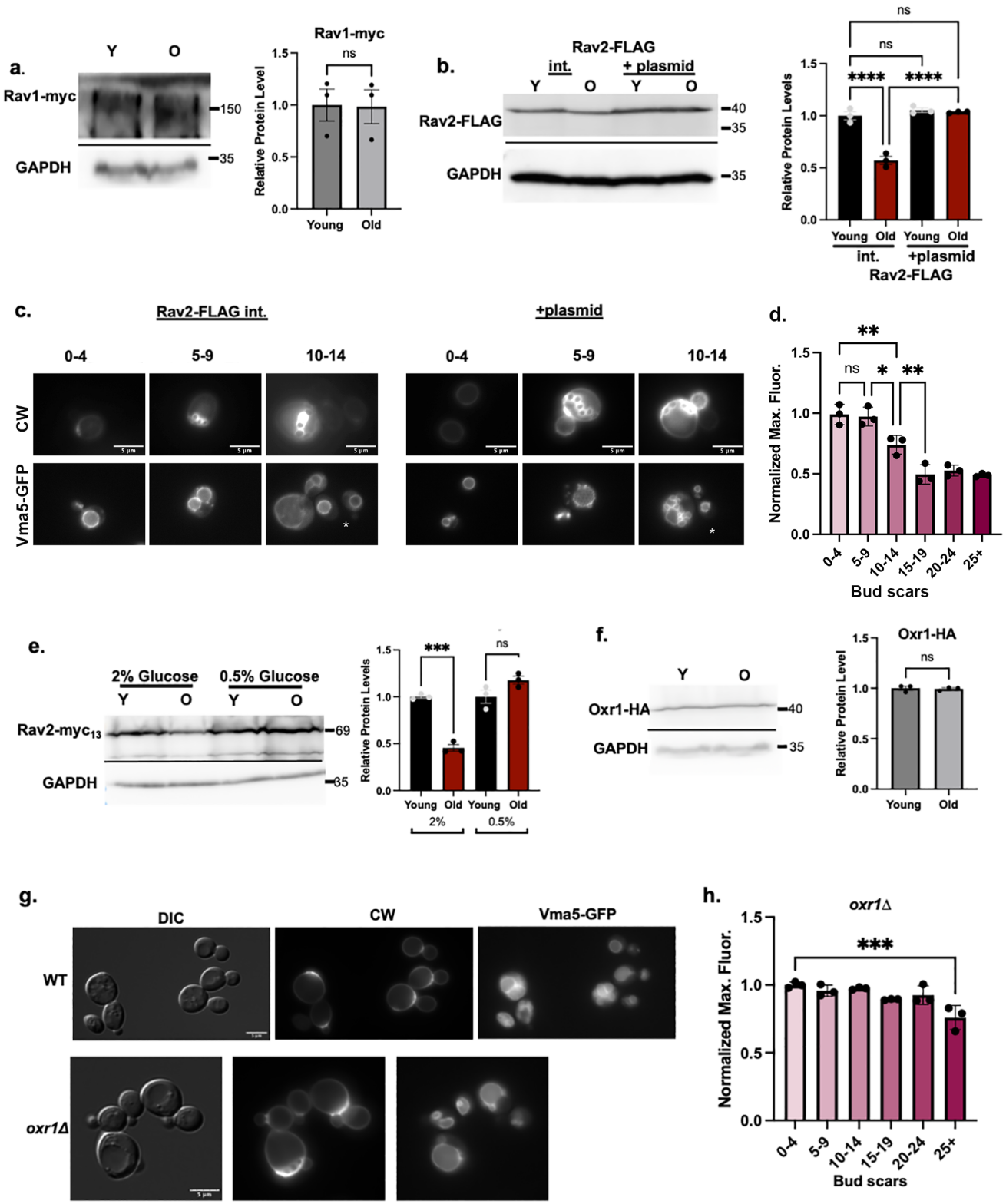
a.
Y
O
Rav1-myc
150
GAPDH
35
Rav1-myc
ns
Relative Protein Level
1.5
1.0
0.5
0.0
Young
Old
b.
Rav2-FLAG
int.
+ plasmid
Y
O
Y
O
Rav2-FLAG
40
35
GAPDH
35
ns
ns
****
****
Relative Protein Levels
Young
Old
Young
Old
int.
+plasmid
Rav2-FLAG
c.
Rav2-FLAG int.
+plasmid
0-4
5-9
10-14
0-4
5-9
10-14
CW
Vma5-GFP
d.
**
ns
*
**
Normalized Max. Fluor.
0-4
5-9
10-14
15-19
20-24
25+
Bud scars
e.
2% Glucose
0.5% Glucose
Y
O
Y
O
Rav2-myc13
69
GAPDH
35
***
ns
Relative Protein Levels
Young
Old
Young
Old
2%
0.5%
f.
Y
O
Oxr1-HA
40
GAPDH
35
Oxr1-HA
ns
Relative Protein Level
Young
Old
g.
DIC
CW
Vma5-GFP
WT
oxr1Δ
h.
oxr1Δ
***
Normalized Max. Fluor.
0-4
5-9
10-14
15-19
20-24
25+
Bud scars